

Atomic Force Microscopy Study of the Adsorption of Surfactant Corrosion Inhibitor Films

Yao Xiong,^{‡*} Bruce Brown,^{*} Brian Kinsella,^{*} Srdjan Nešić,^{*} and Alain Paillet^{**}

ABSTRACT

The properties of an adsorbed corrosion inhibitor—tall oil fatty acid (TOFA) imidazolium chloride—on mica, gold, and X65 steel were studied using in situ atomic force microscopy (AFM). Topography images and thickness measurements show that the structure of inhibitor film changes from monolayer to bi-layer as inhibitor concentration exceeds its critical micelle concentration (CMC). Further kinetic study indicates that the developing of a full film took about 6 h. Quantitative force measurements were performed to evaluate the forces associated with adsorption of inhibitor films. Results show that the mechanical stress needed to physically remove adsorbed inhibitor molecules is of the order of MPa.

KEY WORDS: adsorption, corrosion inhibitor, film, in situ atomic force microscopy

INTRODUCTION

Surfactant corrosion inhibitors can retard acidic corrosion when added to the aqueous environment in very small concentrations (ppm level). Nitrogen-based organic molecules, such as imidazolines, imidazoline amido amines, and their salts, have been widely used as corrosion inhibitors for protecting mild steel from carbon dioxide (CO₂) corrosion.¹⁻⁴ One of the most

important properties of surfactant-type corrosion inhibitors is their ability to adsorb onto a metal surface to form a protective layer.⁵⁻⁷ Understanding the adsorption mechanism and strength of these layers is one critical step leading to better understanding of how they perform their corrosion protection function. It is also an important factor when evaluating and selecting an inhibitor for a field application, and when developing models of corrosion in the presence of inhibitors.

Over the last few decades, the adsorption characteristics of a wide variety of surfactants have been investigated, using calorimetry,⁸⁻⁹ fluorescence decay,¹⁰⁻¹¹ neutron reflection,¹²⁻¹³ and atomic force microscopy.¹⁴⁻¹⁸ One important property of a surfactant is its critical micelle concentration (CMC), which is the concentration when the surfactant molecules spontaneously agglomerate together to form small colloid particles called micelles within the bulk liquid. The micelles significantly affect the adsorption structure of surfactant inhibitors at solid/liquid interfaces and their performance.¹⁹⁻²⁰ A previous study of surfactant adsorption reported that the formation of a first adsorbed layer was due to electrostatic interactions of positive ions on negatively charged surfaces. The second layer is formed with a further increase in surfactant concentration close to the CMC. In this “bi-layer” arrangement, the hydrocarbon “tails” of the inhibitor molecules are facing each other (inward) while the hydrophilic groups point outward—toward the solution and the steel surface.^{6,11,21-22} Other adsorption structures are found above the CMC, such as micelles, hemimicelles, and admicelles, and have also

Submitted for publication: January 1, 2013. Revised and accepted: September 5, 2013. Preprint available online: October 1, 2013. doi: <http://dx.doi.org/10.5006/0915>. Presented as paper no. 2521 at CORROSION 2013, March 2013, Orlando, Florida.

[‡] Corresponding author. E-mail: xiongy@ohio.edu.

^{*} Institute for Corrosion Multiphase Technology, Ohio University, 342 West State Street, Athens, OH 45701.

^{**} Laboratoire Interfaces et Systèmes Electrochimiques, UPMC University Paris VI, UPR 15, 4 Place Jussieu, F-75005 Paris, France.

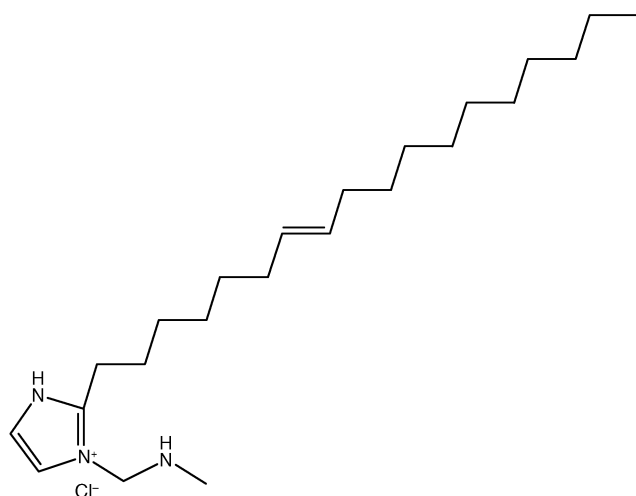


FIGURE 1. Molecular structure of corrosion inhibitor TOFA imidazolium chloride.

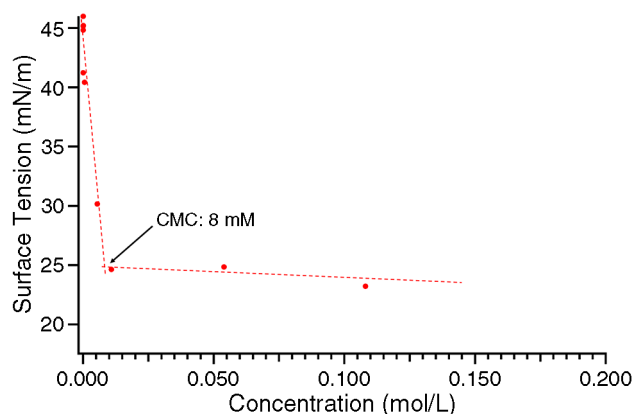


FIGURE 2. Surface tensions of TOFA imidazolium chloride measured at its various concentrations. The CMC for TOFA imidazolium chloride was determined at 8 mM.

been reported for various surfactants.²³⁻²⁵ It has been found that the adsorption and aggregation structures of corrosion inhibitors may vary due to changes in the type of molecules, pH, temperature, counterions, and surface properties of the substrate.²⁶⁻³⁰

Nevertheless, some adsorption properties of corrosion inhibitor films, such as film thickness, mechanical integrity, and adhesion strength, have not been satisfactorily resolved. Studying these properties is very important for understanding the stability and integrity of adsorbed inhibitor films in corrosive environments. A main driver for this work is the widespread discussion about whether inhibitor films can be removed from the metal surface at some critical fluid velocity.³¹⁻³³ This velocity apparently depends on the concentration and type of corrosion inhibitor and is manifested by a rapid increase in the corrosion

rate when inhibitor molecules are removed from the surface. Schmitt, et al., reported that the performance of inhibitor films decreased when the flow velocity exceeded a critical value, suggesting that a high wall shear stress can cause the removal of inhibitor film and inhibition failure.³⁴ Among many others, Zheng, et al., also claimed that high shear stress flow can remove inhibitor layers and significantly decrease their efficiency.³² However, other well-controlled studies have shown that the film integrity was not affected by a high wall shear stress and intense near-wall turbulence.³⁵ Therefore, the resolution of these contradicting findings could only be found by directly measuring the magnitude of the adhesion forces between the steel surface and the inhibitor film and comparing it to the typical hydrodynamic forces seen in the field.

Since the invention of atomic force microscopy (AFM) in 1986,³⁶ great advances have been made in the application of this technique. AFM has the advantage and capability of being able to measure the forces of molecular interaction and adsorption at surfaces. In this work, an in situ AFM was applied to resolve the structure of the adsorbed inhibitor film, to evaluate the mechanical properties of the film, and to determine the stress values needed to remove the inhibitor molecules from the surface.

EXPERIMENTAL PROCEDURES

Materials

The molecular structure of corrosion inhibitor tall oil fatty acid (TOFA) imidazolium chloride is shown in Figure 1. As a 2 nm long cationic surfactant inhibitor, it has a positively charged hydrophilic head and a hydrophobic tail. These molecules can adsorb onto a metal surface and markedly change the corrosion-resistant properties of the metal.³⁷⁻³⁹

The CMC of TOFA imidazolium chloride (Figure 2) was obtained by measuring changes in surface tension with concentration using the drop weight method.⁴⁰ All solutions were prepared using deionized water with a conductivity of 18 $\mu\text{S cm}^{-1}$. The CMC was determined to be 8 mM at pH 4.8 and 25°C.

Mica substrate was first used to develop the AFM techniques for measuring adsorbed film thickness, normal penetration force, and lateral removal force, because it can provide an atomically flat, chemically stable, and negatively charged surface for inhibitor adsorption, making AFM scanning comparatively easy to do and interpret. Subsequent measurements were made on the surfaces of gold (Au) and mild steel. The gold surface was prepared by vapor deposition of gold, under high vacuum, onto a polished Type 316 (UNS S31600)⁽¹⁾ stainless steel substrate. The steel specimen was cut from a pipeline sample of API 5L X65 carbon steel, successively polished using 400, 600, 800, 1,000, and 1,500 grit silicon carbide paper followed by 9, 3, and 1 μm diamond suspensions. For

⁽¹⁾ UNS numbers are listed in *Metals and Alloys in the Unified Numbering System*, published by the Society of Automotive Engineers (SAE International) and cosponsored by ASTM International.

analysis carried out on the steel surface, both the AFM chamber and the inhibitor solution were deoxygenated using CO_2 to eliminate the interference by oxygen corrosion.

Atomic Force Microscopy Measurements

For AFM measurements, aqueous solutions of corrosion inhibitor were prepared at concentrations of 0.5 and 2 times the CMC (i.e., 4 mM and 16 mM, respectively). A freshly cleaved mica, vapor-deposited gold, or polished steel substrate was immobilized in a fluid cell, and the cell was assembled in the AFM instrument with the AFM tip positioned above the substrate surface. Aqueous solution was slowly injected into the cell through the side tubing. Inhibitor film was allowed to fully develop on the surface for a period exceeding 6 h, an optimized duration justified later in this paper. AFM measurements were then carried out in aqueous solutions at the solid-liquid interface to obtain surface morphology,^{14,18} film thickness,⁴¹ penetration force,²⁴ and lateral force measurements.⁴² The scan rate for imaging and lateral force measurements was set to $1,000 \text{ nm}\cdot\text{s}^{-1}$. Typical resolution of 256 by 256 pixels was set in AFM images. No effects of scan rate ($500 \text{ nm}\cdot\text{s}^{-1}$ to $3,000 \text{ nm}\cdot\text{s}^{-1}$) and resolution (up to 512×512) have been found on AFM analysis in this work.

The AFM tips are made of Si_3N_4 and mounted on triangular cantilevers with an average spring constant of 0.4 N m^{-1} . They are known to have a rather hydrophobic character, and their low spring constant was chosen to help maintain the integrity of the inhibitor film during scanning in aqueous solutions. To image the topography of the adsorbed molecular structure, a low normal force ($<2 \text{ nN}$) was applied to the AFM cantilever, which provides a necessary load for imaging and still avoids damaging the delicate inhibitor film structure.

The method to measure film thickness was to first scratch away a small section of the inhibitor film by lateral sweeps (all the way to the original substrate surface) and then image and measure the height difference between the scratched and untouched areas. To investigate the forces required for scratching away adsorbed inhibitor molecules, the normal force applied to the cantilever was gradually increased until lateral cantilever movement was able to remove inhibitor molecules from the substrate surface. The minimal normal force to achieve the removal of adsorbed inhibitor molecules from the various substrate surfaces was determined to be 60 nN . In the first step of this procedure, an XY lateral scan was performed on an area of $1 \text{ by } 1 \mu\text{m}^2$ while still maintaining a high normal force of $\geq 60 \text{ nN}$. In the second step, a portion of the surface slightly larger than the scratched area was imaged using again a low normal force ($<2 \text{ nN}$) to characterize the damage created by the first step. In addition, a line scan, using this low normal force,

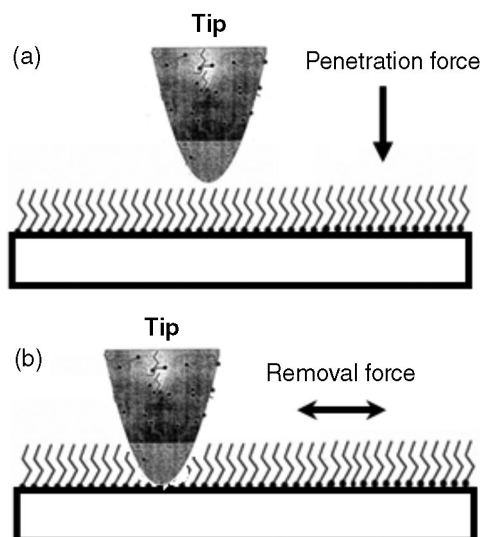


FIGURE 3. Schematic diagrams of (a) the penetration force measurement and (b) the lateral removal force measurement.

traversing the unscratched and scratched areas, was used to determine film thickness in a slightly different way.

The penetration forces determined in this study were obtained using force-distance curve measurements. They were carried out in situ within the inhibited aqueous solution and consist of recording the tip-sample interaction as a function of tip-sample distance when the tip is moved perpendicularly to the surface (Figure 3[a]). Measurements of the lateral force to scratch away inhibitor molecules from substrate surfaces were made using the in situ friction loop technique. This involved a forward and reverse line scan parallel to the surface and perpendicular to the long axis of the AFM cantilever, under an optimized normal load (Figure 3[b]). The optimized normal load was 60 nN and was the same as that used for the film thickness measurements. Using the same normal force in each friction loop allows direct comparison between measurements.

The above procedures to study surfactant corrosion inhibitor films were repeatedly conducted using two different AFM: one instrument located at the Institute for Corrosion Multiphase Technology at Ohio University, and the other one located at the University Paris VI in France. Each analysis, including topography scan, film thickness measurement, and force measurement, has also been performed at least three times to confirm the repeatability and validity of data.

Corrosion Measurements

Corrosion measurements were conducted in a 2-L glass cell setup that contained a three-electrode configuration.³⁵ Test solutions were prepared by dissolving 3% sodium chloride (NaCl) in deionized water, and further deoxygenated by continuous CO_2 bub-

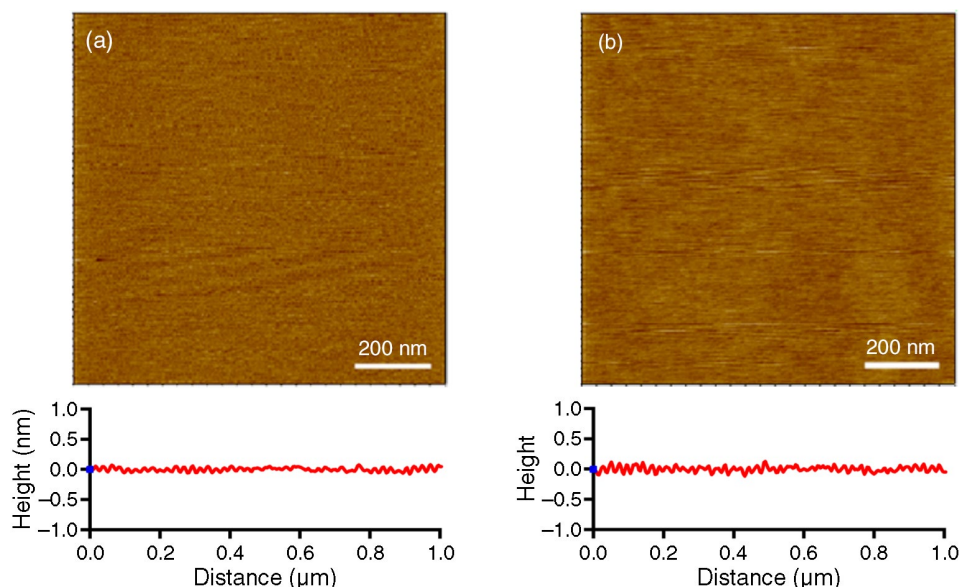


FIGURE 4. Topography images and surface profiles of inhibitor films formed on mica at (a) 0.5 CMC and (b) 2 CMC. The surface roughnesses at both conditions are less than 1 nm.

bling at 1 bar pressure. Solution pH was adjusted to 4.8 using sodium bicarbonate (NaHCO_3), and temperature was maintained at $25 \pm 1^\circ\text{C}$. Cylindrical working electrode was machined from X65 carbon steel with a surface area of 4.94 cm^2 , and mounted on a polytetrafluoroethylene-coated steel rod. Prior to immersion, the working electrode was polished with 400 grit and 600 grit silicon carbide papers, degreased in isopropyl alcohol in an ultrasonic bath, and dried in nitrogen flow. The counter electrode was a ring-shaped platinum (Pt) wire surrounding the working electrode, and the silver/silver chloride (Ag/AgCl; saturated potassium chloride [KCl]) reference electrode was located in a Luggin capillary close to the working electrode.

Corrosion rates were monitored by linear polarization resistance (LPR) programmed in a potentiostat. LPR measurements were performed in a range of $\pm 5 \text{ mV}$ with respect to the open-circuit potential and a scan rate of 0.125 mV/s during each test to maintain a deoxygenated environment. A "B" constant value of 23 mV was used to calculate corrosion rate from measured polarization resistance.⁴³ TOFA imidazolium chloride was injected into the glass cell 2 h after reaching the stable baseline corrosion rate.

RESULTS AND DISCUSSION

Measurements on Mica

Adsorption Structure and Film Thickness — Figures 4(a) and (b) show surface morphologies of thin films adsorbed on mica from aqueous TOFA imidazolium chloride solutions containing 0.5 and 2 times the CMC, respectively. The topography images were obtained over an area of $1 \text{ by } 1 \mu\text{m}^2$. The surface profile plots show that the full z-scale in both conditions is

less than 2 Angstroms. The uniform featureless surfaces shown in these images suggest that the inhibitor molecules are adsorbed at the mica/solution interface as a continuous (pinhole-free) film, flat on an atomic scale. This is regardless of the internal structure of the film, which could vary. No artifacts are shown in the images, indicating that the adsorbed structure was not disrupted by the scanning process. Multiple images on different locations of the surface confirmed that the mica/solution interface was fully covered by a flat inhibitor film at concentrations of both 0.5 and 2 times the CMC.

To investigate the internal structure of the inhibitor films and to accurately measure film thickness, the inhibitor molecules were removed by scratching the surface over an area of $1 \text{ by } 1 \mu\text{m}^2$. Figure 5 shows AFM images produced after the scratching in which the central areas are those where different applied normal forces were used in attempts to remove the inhibitor molecules by the AFM tip. The same tip was used in the three experiments shown in Figure 5, to maintain consistent conditions. When the applied normal force was $< 2 \text{ nN}$, i.e., less than the critical force for the tip to penetrate the inhibitor film, the image revealed the surface morphology of the adsorbed inhibitor (Figure 5[a]). When the normal force was set to 40 nN , the tip was able to penetrate the inhibitor film and create features shown in Figure 5(b). However, because the force was insufficient to remove molecules from the surface, the inhibitor film appears to be more or less intact after the scratching procedure. When the applied normal force was set to 60 nN , the inhibitor molecules were removed from the scratched area, as shown in the center of the image in Figure 5(c). Further increases in the applied normal

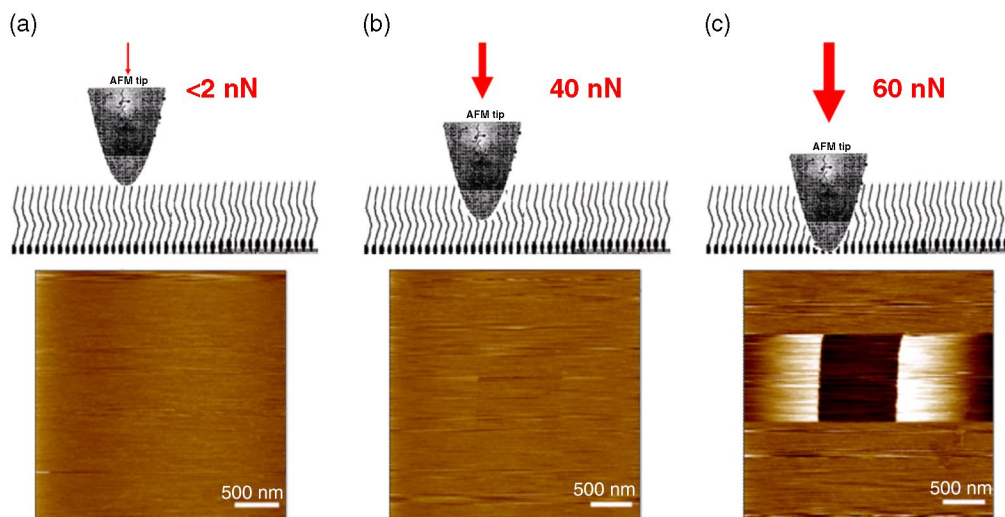


FIGURE 5. Topography images of inhibitor films formed at 2 CMC and scanned using different normal forces applied to the cantilever: (a) $< 2\text{ nN}$, (b) 40 nN , and (c) 60 nN . Each of these images is accompanied with a schematic diagram showing the AFM tip-inhibitor film interaction.

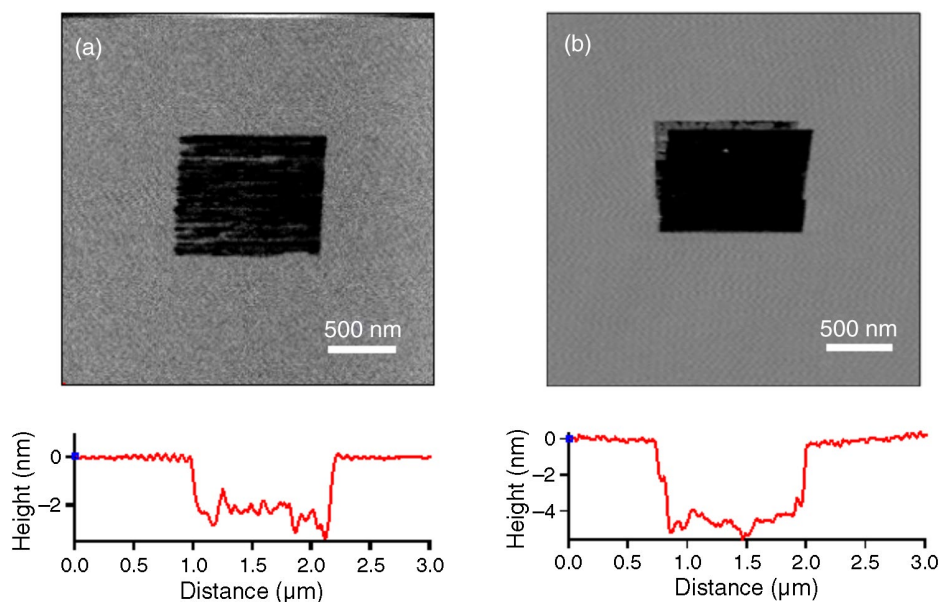


FIGURE 6. Film thickness measurements for TOFA imidazolium chloride on the mica surface at concentrations of (a) 0.5 CMC and (b) 2 CMC. The film thickness was determined by measuring the height difference between scratched and unscratched areas. The 2 nm and 4 nm depths at 0.5 CMC and 2 CMC conditions correspond to the monolayer and bilayer structures, respectively.

force beyond 60 nN did not change the depth of the scratched area since the underlying, much harder mica surface was not scratched by the tip. Figure 6 shows the AFM images of the area after scratching, in 0.5 CMC and 2 CMC inhibitor solutions, respectively. Line scans taken across the scratching prints show depths of 2 nm and 4 nm at 0.5 CMC and 2 CMC, respectively, which approximately corresponds to one and two TOFA imidazolium chloride molecular lengths. That is, it appears that a mono-molecular layer is formed at 0.5 CMC and a bi-layer at 2 CMC,

which is consistent with models proposed in some previous publications.^{6,15,44} The film thickness measurements of 2 nm and 4 nm were consistent when scratching was repeated in different areas on the mica surface, indicating that a continuous, uniform, adsorbed film had formed over the surface in both cases. The experiment was repeated many times with the same result. To confirm that the measured film thickness was due to adsorbed surfactant molecules, similar experiments were repeated in pure water in the absence of TOFA imidazolium chloride. The images

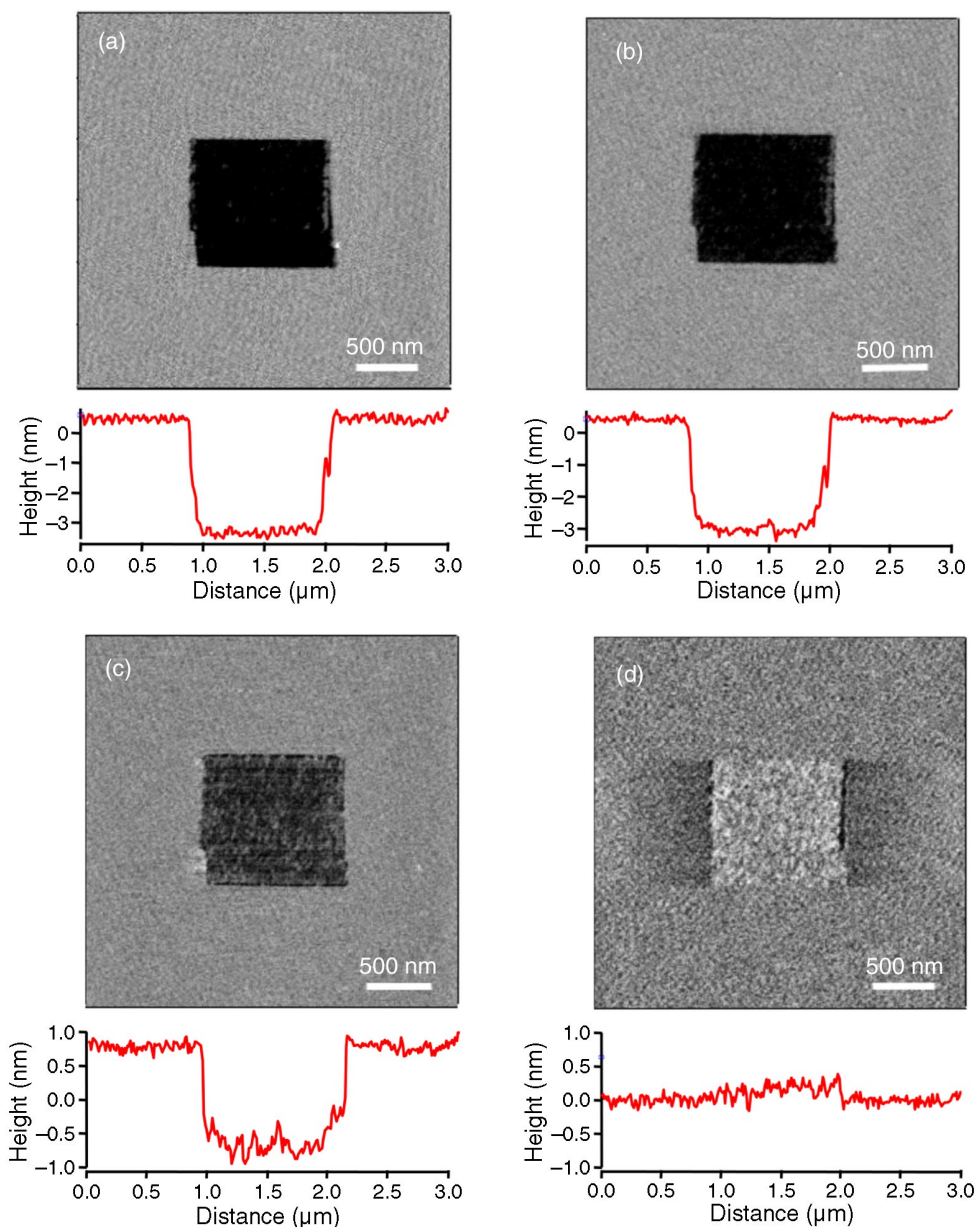


FIGURE 7. Topography images and surface profiles of an area (a) immediately, (b) 1 h, (c) 3 h, and (d) 6 h after film removal. The scratched area was gradually restored by inhibitor molecules in 6 h.

revealed a uniform, featureless surface and no effect of scratching could be detected.

Kinetics of Readsorption — An obvious question that emerged following these film thickness measurements was: Why did the inhibitor molecules not re-adsorb after being scratched away from the surface? It was hypothesized that the kinetics of readsorption was relatively slow. A new series of experiments was conducted and profile measurements taken at different time intervals after scratching away the inhibitor molecules in a 2 CMC solution. Figure 7 shows topography images and profiles following the inhibitor layer removal by scratching in the central area, as described above. The depth of the scratched area

was 4 nm at the beginning, immediately following the removal process (Figure 7[a]), corresponding to the thickness of a bilayer film. The scratched area was gradually “restored” (Figures 7[b] and [c]) as the inhibitor re-adsorbed, and it appears fully covered by inhibitor molecules after 6 h (Figure 7[d]). These data explain why at least 6 h was used to obtain a full layer of adsorbed inhibitor on mica, before any measurements were done, as described in the “Experimental Procedures” section. It also demonstrates the ability of the AFM technique to characterize the kinetics of inhibitor film formation, which is important information for any modeling purposes as well as for many practical applications such as inhibitor batch

treatment and in cases where pigging or sand production operations can temporarily destroy the inhibitor film on pipe surfaces.

Penetration Force Measurements — Although it is not fully understood how protective inhibitor films form, the effectiveness of the film to reduce corrosion could be generally related to molecular size (length), film thickness, and packing density of the adsorbed inhibitor molecules.⁴⁵⁻⁴⁷ The integrity and persistence of the inhibitor film in flowing solutions is also of paramount importance in pipeline situations. In this section it is described how some mechanical properties of an inhibitor film were evaluated using AFM force-distance measurements. Figure 8 shows force-distance curves measured on inhibitor films formed on mica from aqueous solutions at 0.5 CMC and 2 CMC solutions. These curves are compared to the curve obtained for bare mica, i.e., mica immersed in pure water in the absence of surfactant inhibitor molecules. The Y axis shows the measured force applied to the AFM tip, and the X axis represents the position of the tip in the direction perpendicular to the surface.

On the bare mica surface, which is free of adsorbed surfactant molecules, the force between the tip and surface is zero when the distance is larger than 2 nm, indicating that there is no interaction of the AFM tip with the surface. When the distance of the tip is approximately 2 nm (see black dotted curve), one can observe a “jump to contact” event, i.e., the tip is suddenly attracted to the surface due to short-range attractive forces, which manifests itself as a negative force in Figure 8. Further downward movement of the AFM tip pushes it against the hard mica surface, and the resulting repulsion exerted on the AFM probe produces a positive force that increases linearly with distance as a result of the flexing of the cantilever and incompressible character of mica substrate. Under these experimental conditions, one can use the linear part of the approach curve to extract the normal angular sensitivity of the AFM tip.

In the presence of surfactant inhibitor films, the tip being initially far from the surface does not interact with it, as illustrated by the zero force measured on the initial part of the curve to the left. As the tip moves downward approaching the surface, it starts interacting with the outer portion of the inhibitor film at a given distance. This interaction is revealed by an increasing positive/repulsive force. It is thought that this force results in an indentation (or compression) of the inhibitor film produced by the AFM tip. This repulsive force reaches a maximum here called “breakthrough” force corresponding to a situation where the tip starts penetrating the inhibitor film. This situation is followed by an abrupt decrease in repulsive force, corresponding to further incursion of the tip inside the film. Further movement of the AFM tip toward the surface causes the force to increase again as the tip is pressed against the incompressible mica surface, as

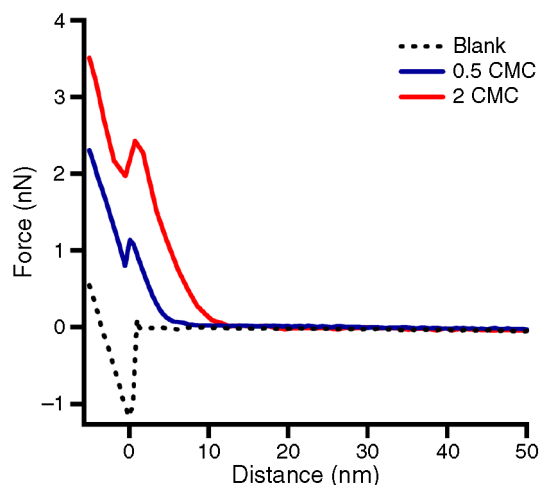


FIGURE 8. Penetration force measurements on mica surface in the absence and presence of corrosion inhibitor TOFA imidazolium chloride.

already observed in the absence of inhibitor film. In the case of the films formed at 0.5 CMC and 2 CMC, the breakthrough force is measured at about 1.1 nN and 2.4 nN, respectively. One can notice that the force required to penetrate the thicker film resulting from a 2 CMC inhibitor concentration is appreciably higher.

Other authors have used this force-curve technique to determine the thickness of adsorbed molecules;⁴⁸ however, while it may provide an indication of inhibitor film thickness within an order of magnitude, it is not considered to be accurate enough. The technique described above of film nano-scratching followed by a line profile measurement gives a more accurate measurement of film thickness. The force-distance measurements when used to determine film thickness usually lead to an overestimation of the film thickness. This is because part of the measurement involves sensing the interaction between the AFM tip and adsorbed inhibitor layer due to Van der Waals type forces, which are sensed further away from the inhibitor surface.

However, the force-distance measurements described above provide valuable information about the force required to penetrate an inhibitor film. The force exerted by the flow of fluid in pipelines is usually expressed in terms of a stress (force/unit area) with units of Pascal (Pa). To roughly compare the AFM penetration force measurements with the forces produced by fluid flow, the AFM measurements were converted into a pressure form (Pa) by dividing by the penetration force with the cross-sectional area (πr^2) of the hemispherical-shaped apex of the AFM tip. The radius of curvature, of ~ 15 nm, was obtained from the high-resolution SEM image of the AFM tip. Using this radius, a cross-sectional area of 7×10^{-16} m² is calculated. The measured penetration forces of 1.1 nN and 2.4 nN can be converted to shear stress of 1.6 MPa

TABLE 1

Summary of Atomic Force Microscopy Measurements for TOFA Imidazolium Chloride Inhibitor Films on Mica, Gold, and X65 Steel Substrates

Substrate and Inhibitor Concentration	Inhibitor Film Thickness (nm)	Penetration Force (nN)	Penetration Stress (MPa)	Removal Force (nN)	Removal Stress (MPa)
Mica	0.5 CMC	2	1.1±0.2	40±7	57±10
	2 CMC	4	2.4±0.2	44±5	63±7
Au	2 CMC	4	0.9±0.3	35±18	50±26
X65 Steel	0.5 CMC	2	1.6±0.3	75±15	107±21
	2 CMC	4	3.1±0.3	75±14	107±20

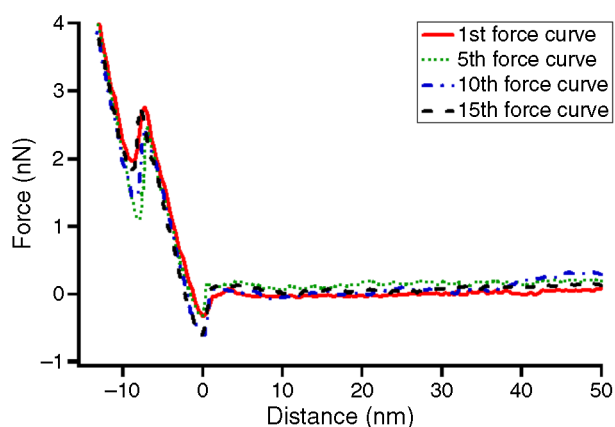


FIGURE 9. Repeated penetration force measurements at the same position on mica surface in a 2 CMC solution of TOFA imidazolium chloride.

and 3.4 MPa, respectively, for inhibitor films formed at 0.5 CMC and 2 CMC (Table 1).

A mechanism for inhibitor failure in flowing solutions has been repeatedly attributed to the wall shear stress removing inhibitor films from steel pipe walls.³¹⁻³⁴ The typical values of shear stress in pipe flow are in the range from 1 Pa to 10 Pa, with fluctuations seen under the most extreme conditions in multiphase slug flow not exceeding 1 kPa.⁴⁹⁻⁵¹ Based on our penetration force measurements, it appears that an MPa level stress is required to break through the inhibitor film. Therefore, from this coarse order-of-magnitude type of comparison, it seems unlikely that realistic fluid flow can physically damage the adsorbed inhibitor film.

However, this comparison can be considered unfair since it involves a force required to penetrate inhibitor films measured perpendicular to the sample surface, whereas the wall shear stress is a result of shearing forces parallel to the surface. In other words, the penetration force is probably related to the mutual interactions between the adsorbed inhibitor molecules and not to the force between the inhibitor molecules and the substrate surface. Furthermore, these measurements were made on mica and not on steel. To

address these concerns, lateral force measurements carried out on mica were then progressed to gold and X65 grade mild steel. The results and discussion of these measurements are given in subsequent sections of this paper.

Interestingly, the normal penetration of the inhibitor film by the AFM tip did not damage the film structure or observably remove any inhibitor molecules. Figure 9 shows repeated, uninterrupted, force-distance penetration curves recorded at the same position on the mica surface. After 15 repeated penetrations, the film appeared still intact as indicated by the similar force/distance curves and mechanical resistance to the AFM tip. This suggests that the penetration only temporarily/elastically “pushed apart” the inhibitor molecules, and when the tip was withdrawn they returned to their original positions with their overall structure intact. AFM images of the area where the penetration measurements were carried out also did not show any defects or damage of the film due to tip penetration. Results suggest that inhibitor molecules remained adsorbed on the surface even when the film was penetrated.

Lateral Removal Force Measurements — While the inhibitor molecules were not removed by AFM tip penetration, removal of inhibitor molecules was achieved by nano-scratching seen during the film thickness measurements as described above, due to the lateral interaction between the tip and the adsorbed molecules. In this section, it is reported how AFM was used to quantitatively measure the magnitude of the lateral force required to remove adsorbed inhibitor molecules from the surface. These types of force measurements more closely relates to the shear force required for removal of the inhibitor molecules from the substrate surface.

The lateral force was measured by applying the minimum required normal force of 60 nN to the cantilever, as described above for the film thickness measurements. Using this force, it was found that the inhibitor molecules could be removed from the surface by the scanning tip (Figures 5 and 6). It was established, moreover, that this normal force is far larger than the breakthrough force (1.1 nN or 2.4 nN). To

perform a lateral force measurement, a cyclic line scan, also called a “friction loop,”⁴² was used. The AFM tip was initially brought into contact with the mica surface at a 60 nN normal force and then it was moved in one direction (forward scan), and then traversed back to the starting point by scanning in the opposite direction (reverse scan). Both scans were done in the direction perpendicular to the length of the cantilever at the same scan speed. A lateral flexing of the cantilever ensured that the forward and reverse scanning did not fully overlap. The AFM instrument records the cantilever torque induced by the lateral interaction between the AFM tip and the sample surface. The lateral spring constant and AFM photodiode lateral sensitivity were used to convert the raw data into quantitative force values. The average lateral sensitivity of 45 nm/V was calibrated by using the AFM operation software. The average lateral spring constant of 36 N/m was calculated using the following equation:⁴²

$$k_{\text{lat}} = \frac{2}{6 \cos^2 \theta + 3(1 + \nu) \sin^2 \theta} \left(\frac{L}{H}\right)^2 k_n \quad (1)$$

where k_{lat} is the lateral spring constant of the cantilever beam, L is its length, H is the height of the tip, k_n is the normal spring constant, θ is the angle between the base arms of the triangular cantilever, and ν is the Poisson ratio for Si_3N_4 .⁴² L , H , and θ were measured using scanning electron microscopy.

Figures 10 and 11 show lateral force measurements for a mono-molecular layer and a bi-molecular layer film formed in 0.5 CMC and 2 CMC solutions, respectively. In each of these figures, there are two sets of friction loops recorded on two different surfaces, one for a mica surface in water (blank) and the other for a mica surface covered with an inhibitor film in an aqueous solution of the inhibitor at the corresponding concentration. The curves were recorded using the same tip, scan speed of 1 Hz, and normal force (60 nN) applied to the cantilever. Positive and negative friction forces shown in the graphs correspond to the force recorded during the forward and reverse scans, respectively. In Figure 10, the average lateral force on inhibitor-free mica was 163 nN, while the average lateral force in the presence of the monolayer inhibitor film (0.5 CMC) was 203 nN. The significant increase in the lateral force of approximately 40 nN is attributed to a change in surface properties and the force to remove adsorbed inhibitor molecules from the mica surface.

In Figure 11, the average lateral force on inhibitor-free mica was 163 nN, while the average lateral force in the presence of the bilayer film (2 CMC) was 207 nN. Correspondingly, the difference of 44 nN is attributed to the lateral force for removing inhibitor molecules away from the mica surface. The lateral force measurements recorded on a bi-layer inhibitor

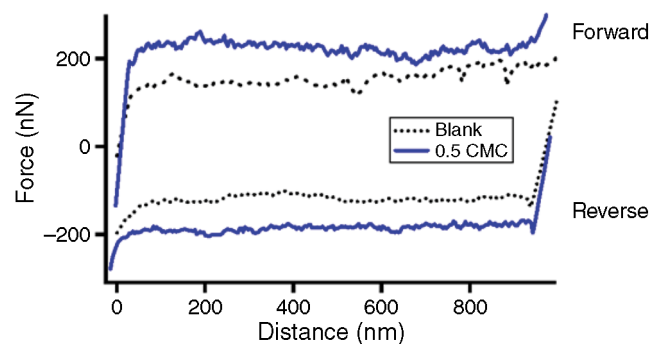


FIGURE 10. Lateral force measurements on mica surface in the absence and presence of a 0.5 CMC solution of TOFA imidazolium chloride.

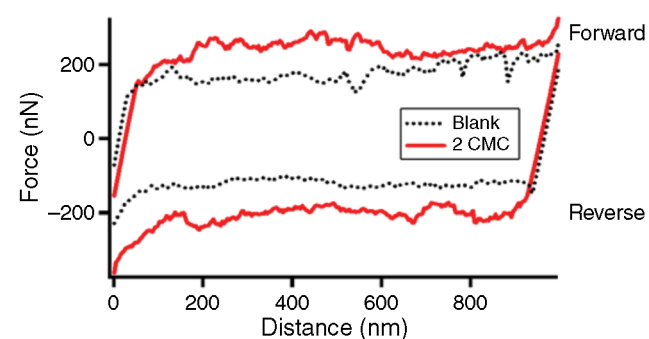


FIGURE 11. Lateral force measurements on mica surface in the absence and presence of a 2 CMC solution of TOFA imidazolium chloride.

film in a solution at 2 CMC are very similar to those obtained with a monolayer film in Figure 10. These results provide evidence that the lateral force was measured by interrupting the interaction between the hydrophilic moiety of adsorbed molecules in the first molecular layer and the mica surface. The second molecular layer, which stacked on top of the first layer, did not contribute to the molecule-to-surface interaction, and thus did not alter the lateral force. Even though a 20% variation can occur during lateral force measurements (Table 1), especially on relatively rougher Au and steel surfaces, our measurements are still valid because we mainly focus on the order of magnitude of calculated shear stress from force measurements.

The lateral force measurements were converted into a shear stress by using the same cross-sectional area of $7 \times 10^{-16} \text{ m}^2$ as in the penetration force measurements (Table 1). It is difficult to know the exact contact area during friction experiments, i.e., the actual area of the tip acting on the inhibitor molecules during lateral movement. Therefore, the values of shear stress in Table 1 (MPa) are only estimated values, but nevertheless suitable for order-of-magnitude comparisons to the wall shear stress produced by fluid flow in pipelines. Table 1 shows the measured

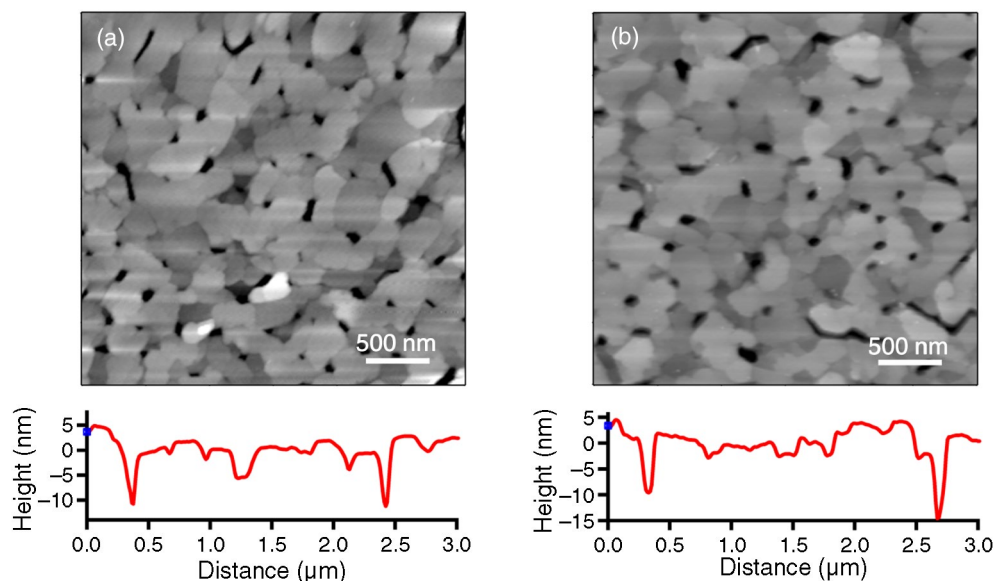


FIGURE 12. AFM topography images and surface profiles on Au surface in (a) deionized water and (b) a 2 CMC solution of TOFA imidazolium chloride.

lateral forces and calculated stress values, and the calculated shear stresses to remove monolayer and bilayer inhibitor films are of the order of 60 MPa. Comparing with the wall shear stress in realistic flow in pipelines,⁴⁹⁻⁵¹ the shear stress required to mechanically remove inhibitor films is at least four orders of magnitude higher than the wall shear stress generated by fluid flow. Even considering the possible error in the estimation of contact area, the measured stress is still orders of magnitude higher than the wall shear stress in a pipe flow.

Table 1 provides a summary of normal and lateral force measurements for monolayer and bi-molecular layer films formed on mica from solutions of TOFA imidazolium chloride at 0.5 and 2 times the CMC. It is emphasized again that in Table 1, the force measurements given in nN, which were obtained by AFM force-distance curves and friction loops, are accurate values, directly determined by AFM force measurements. The numbers for shear stress, in MPa, are calculated values based on the measured forces and the estimated cross-sectional area of the AFM tip. It can be seen that the lateral force is independent of film thickness and inhibitor concentration, indicating this force is only related to the adsorption between inhibitor hydrophilic groups and mica surface. For a given inhibitor molecule, its adsorption strength on the surface does not change when there are more adsorbed layers. And the measured lateral force is at least 20 times greater than the corresponding penetration force, indicating it is much harder to physically remove adsorbed molecules than to penetrate through the film structure. In other words, the inhibitor-surface force interactions are, in this case, much stronger than the inhibitor-inhibitor interactions.

Measurements on Gold

To investigate whether the penetration and removal forces measured on mica are typical of other more practical materials, similar experiments and measurements to those reported above were performed on gold and steel substrates. The measurements for steel are described in the following section. Studies on gold were carried out first because the testing environment was non-corrosive to gold. Investigations of inhibitor film formation on several substrates helped answer questions such as:

- Is the morphology of the inhibitor films similar?
- Does the normal penetration and lateral removal forces change with different substrates?

AFM images of a vapor-deposited gold surface in the absence and presence of TOFA imidazoline at 2 CMC are given in Figure 12. It can be seen from this figure that the Au surface is comparatively rough with a peak-to-peak roughness of 20 nm, and the presence of the inhibitor did not change or significantly affect surface morphology. This indicates that inhibitor molecules formed a continuous flat film on gold surface, similarly as on mica. The corresponding penetration force measurements for these surfaces are given in Figure 13. Despite the apparent lack of influence on surface morphology, the inhibitor has had an obvious effect on the force distance curve. With no inhibitor present, a negative attractive curve was recorded, but in the presence of inhibitor at 2 CMC, a positive repulsive force is obtained. The force to penetrate the inhibitor film is about 2 nN, which is similar to the result for a bimolecular layer film formed on mica.

Lateral removal force measurements were conducted, first, to estimate the thickness of the film, and, second, to estimate the strength of adsorption.

These measurements were performed using a normal load of 60 nN, the same as the load used for mica. An AFM image of the film thickness and surface profile is shown in Figure 14. Figure 15 shows the lateral force measurements for Au in water and in the presence of 2 CMC, TOFA imidazolium chloride. Despite the surface roughness causing interference with the film thickness measurement, the results are comparable to those recorded for mica (Table 1).

Measurements on X65 Steel

The work described above using an atomically smooth mica surface and a rougher gold surface naturally progressed to carrying out similar measurements on a mild steel substrate. Imaging of surfactant molecules adsorbed on steel by AFM has been reported earlier by Bosenberg, et al.⁵² In that investigation, the structure of inhibitor molecules adsorbed on steel were similar to those imaged on mica, but no attempt was made to measure film thickness or the mechanical and adsorption properties of the film.

Adsorption Structure and Film Thickness — Figure 16 shows the topography images and surface profiles of highly polished X65 grade steel in deionized water and aqueous solutions of TOFA imidazolium chloride at concentrations of 0.5 CMC and 2 CMC. These images were obtained from three different locations on the X65 surface, and thus the orientations of polishing marks are different. After the polishing, the peak-to-peak roughness of steel surface is less than 10 nm (Figure 16[a]), which makes it eligible for AFM analysis. Further adsorption of inhibitor films (Figures 16[b] and [c]) did not change the surface roughness and surface features. This indicates that the adsorption of inhibitor molecules follows the original morphology of the steel surface, and continuous flat inhibitor films were formed at both 0.5 CMC and 2 CMC conditions.

Film thickness was measured for inhibitor films using the previously described procedure. Figure 17 shows that the film thickness is 2 nm and 4 nm for films formed at 0.5 CMC and 2 CMC, respectively, corresponding to the monolayer and bimolecular layer film formation at respective inhibitor concentrations. These results are consistent with those obtained on mica substrates, indicating this type of inhibitor has similar adsorption properties on mica and steel surfaces.

Penetration Force Measurements — Figure 18 shows force distance curves, using X65 grade steel as the substrate, in deionized water and in the presence of inhibitor films formed at 0.5 CMC and 2 CMC. The force to penetrate the inhibitor films are given in Table 1. Table 1 also provides a summary of the penetration force and lateral removal force measurements recorded at different inhibitor film thicknesses for mica, gold, and X65 grade steel. It can be seen that the shape of the curves using X65 grade steel

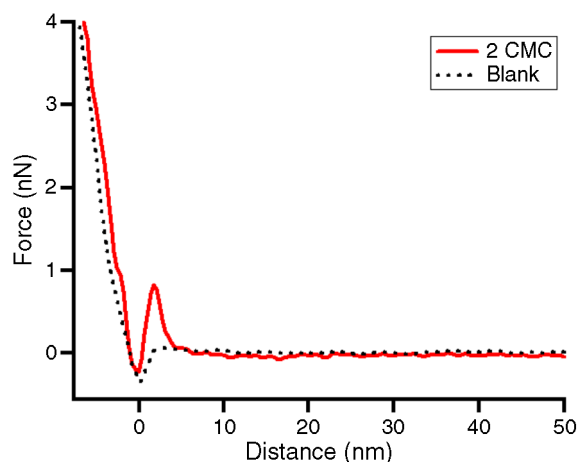


FIGURE 13. Penetration force measurement on the Au surface in the absence and presence of corrosion inhibitor TOFA imidazolium chloride.

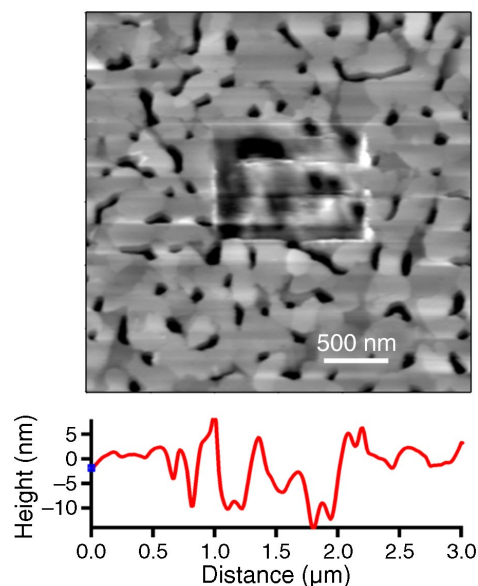


FIGURE 14. Film thickness measurement of on a Au surface in a 2 CMC solution of TOFA imidazolium chloride.

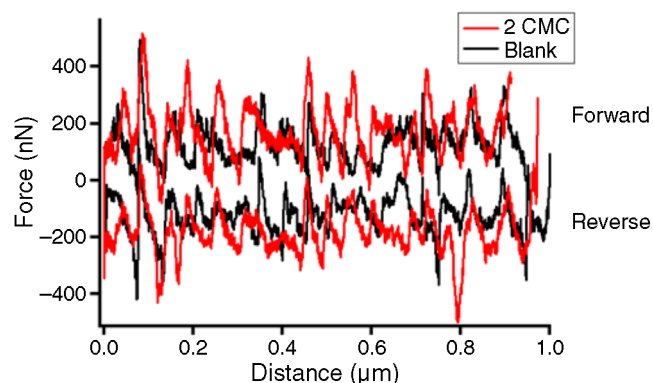


FIGURE 15. Lateral force measurements on a Au surface in a 2 CMC solution of TOFA imidazolium chloride.

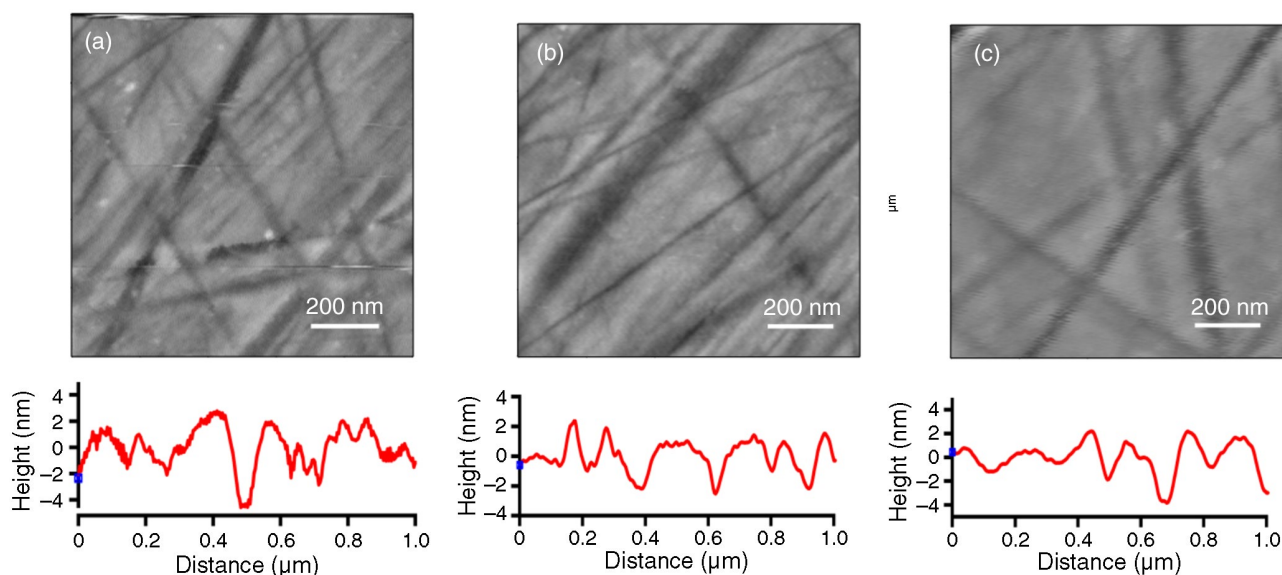


FIGURE 16. AFM topography images and surface profiles of polished X65 steel surface in (a) deionized water, (b) 0.5 CMC, and (c) 2 CMC solutions of TOFA imidazolium chloride.

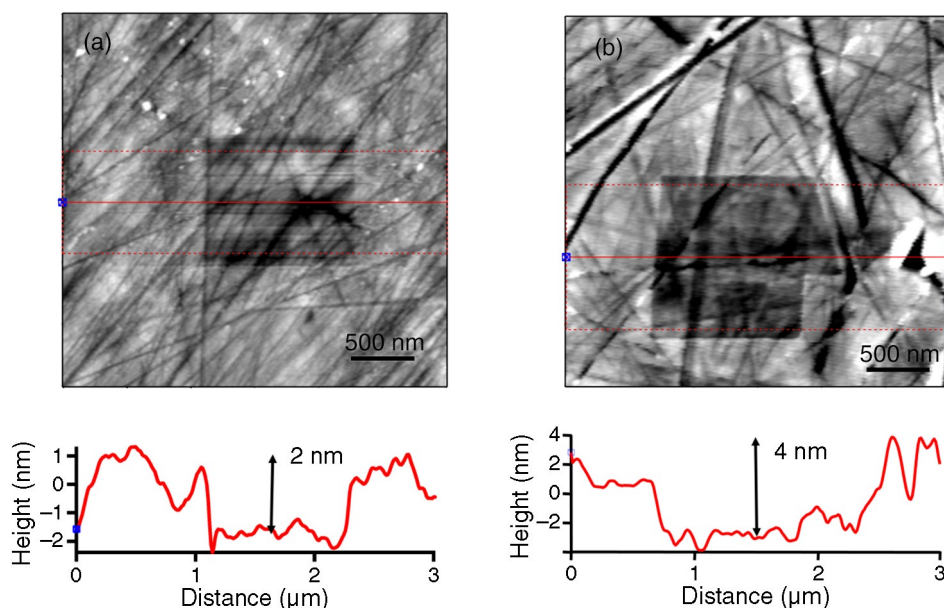


FIGURE 17. Film thickness measurements for TOFA imidazolium chloride on X65 steel surface at concentrations of (a) 0.5 CMC and (b) 2 CMC.

as a substrate are similar to those obtained using a mica substrate. The presence of an inhibitor film has significantly changed the shape of the force-distance curves compared to the blank. The force to penetrate the bimolecular layer film, formed at 2 CMC, is about 3 nN and is twice the force to penetrate the monomolecular layer film formed at 0.5 CMC. These results are also consistent with the forces recorded on the mica substrate.

Lateral Removal Force Measurements — Figure 19 shows the friction loop curves for monolayer and bimolecular layer films of TOFA imidazolium chloride on

X65 steel in solutions at 0.5 CMC and 2 CMC. These curves are compared to the friction loop curve for X65 steel in deionized water with no inhibitor present.

The technique was the same as that used for mica with a normal load of 60 nN applied to the cantilever. The lateral removal force for the surfactant molecules was determined from the difference in the two curves, i.e., by subtracting the average force in the presence of an inhibitor film from the average force obtained with no inhibitor film present. The removal force was determined to be about 75 nN for both the mono and bimolecular layer films. As anticipated, the results

are independent of film thickness since they are a measurement of the force between the molecules' hydrophilic head group and the substrate surface. Comparing with the forces on mica and gold substrates, the lateral removal forces measured on the steel surface are much higher (Table 1). This is because the imidazoline ring, which is "rich" in electrons, is able to share electrons with Fe atoms and lead to stronger interactions.⁵³⁻⁵⁴ By further converting these lateral force values to stress values, based on the cross-sectional area of the AFM tip, the stress to physically remove inhibitor molecules is as high as 100 MPa. Even considering the possible variations in the tip area during the scanning, and other uncertainty involved in the calculations, one can conclude that the stress value required to remove inhibitor film from the steel surface is in the MPa range. These results indicate that the realistic fluid flow found in pipelines, where wall shear stress does not exceed 1 kPa, cannot cause mechanical removal of inhibitors from a mild steel surface and increased corrosion.

Corrosion Rate Measurements

To better relate corrosion inhibitor performance to the AFM measurements, particularly for the case of X65 steel, corrosion rate measurements were conducted for X65 steel in CO₂-saturated environments at TOFA imidazolium chloride concentrations of 0.5 and 2 times the CMC. Figure 20 shows corrosion rate versus time measurements for the two inhibitor concentrations. In both cases, the initial corrosion rate was high and reduced to lower rates due to the presence of the inhibitor. It took 5 h to 6 h to achieve a steady-state corrosion rate and maximum level of protection. This time is similar to the time detected by AFM for the inhibitor film to readsorb on mica. The higher steady-state corrosion rate of 0.26 mm/y obtained at an inhibitor concentration of 0.5 CMC can be attributed to the formation of a less protective mono-molecular layer film. On the other hand, the lower corrosion rate of 0.05 mm/y, at an inhibitor concentration of 2 CMC, can be attributed to the formation of a more protective bimolecular layer film as proven by the AFM measurements.

CONCLUSIONS

❖ It was found that TOFA imidazolium chloride inhibitor films formed a continuous and uniform film on mica, gold, and X65 grade steel surfaces. The measurements indicated that a monolayer formed below the CMC, i.e., at 0.5 CMC, while a bi-layer formed above the CMC, i.e., at 2 CMC.

❖ AFM measurement of the force used to penetrate the inhibitor films is related to film structure. A significantly greater force was required to penetrate bi-layer than monolayer films but both were found to be about 20 to 40 times lower than the force required to

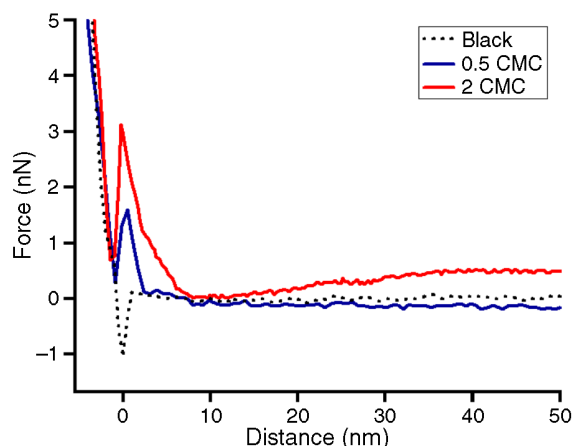


FIGURE 18. Penetration force measurements on X65 steel surface in the absence and presence of TOFA imidazolium chloride.

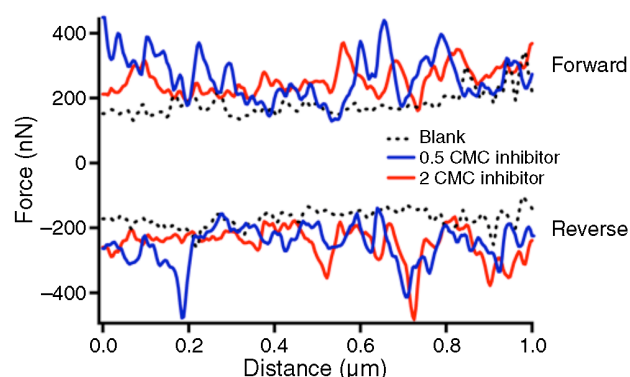


FIGURE 19. Lateral force measurements on X65 steel surface in the absence and presence of TOFA imidazolium chloride.

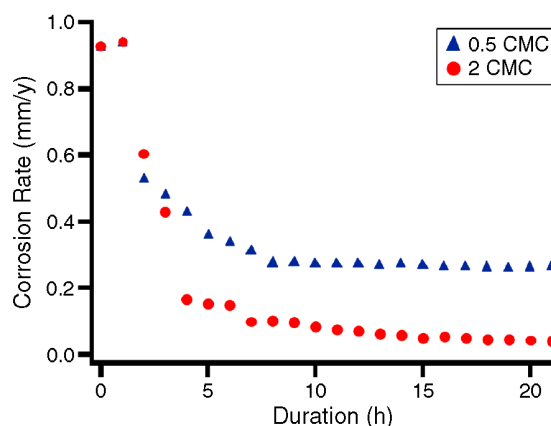


FIGURE 20. Corrosion rates were measured on X65 steel specimens in 0.5 CMC and 2 CMC solutions of TOFA imidazolium chloride. In both conditions, the corrosion rate reached a steady state after adding inhibitors for 5 h to 6 h.

remove the inhibitor films from the substrate surface in nano-scratching tests. Lateral removal force measurement in nano-scratching tests is directly related to the strength of adsorption between the inhibitor

molecule hydrophilic group and the substrate surface and not to the number of inhibitor molecular layers, because these measurements were independent of film thickness.

❖ The shear stress required to remove inhibitor molecules from the surface determined by AFM lateral force measurements was 50 MPa to 100 MPa, which is at least three orders of magnitude above the maximum shear stress obtained by realistic fluid flow in pipelines (<1 kPa), even under the most severe hydrodynamic conditions. Therefore, it is unlikely that this type of inhibitor film can be removed from mild steel pipe walls as a result of shear forces produced by fluid flow.

❖ It is recognized that an appreciable error may be involved in converting lateral AFM force measurements to a shear stress due to the uncertainty of knowing the actual area of the AFM tip interacting with the adsorbed molecules in the inhibitor film. Nevertheless, because of the many orders of magnitude in difference between the AFM-determined shear stress and the hydrodynamic wall shear stresses seen in practice, the above conclusion is still considered valid.

ACKNOWLEDGMENTS

C. Deslouis (LISE, UPR 15 of CNRS) and Liwei Chen (SINANO, Chinese Academy of Sciences) are acknowledged for fruitful discussions. The International Relations Office of Univ. P. & M. Curie (Paris, France) is acknowledged for the financial support of the collaboration between LISE and ICMT (Athens, Ohio, Ohio University).

REFERENCES

1. Y. Duda, R. Govea-Rueda, M. Galicia, H.I. Beltran, L.S. Zamudio-Rivera, *J. Phys. Chem. B* 109 (2005): p. 22674-22684.
2. E. Garcia-Ochoa, J. Cruz, R. Martinez, J. Genesca, *J. Electroanal. Chem.* 566 (2004): p. 111-121.
3. M. Du, F.G. Liu, J. Zhang, M. Qiu, *Corros. Sci.* 51 (2009): p. 102-109.
4. Z. Jun, J.X. Liu, W.Z. Yu, S.G. Hu, Y. Long, G.M. Qiao, *Appl. Surf. Sci.* 256 (2010): p. 4729-4733.
5. M.J. Rosen, *Surfactants and Interfacial Phenomena*, 3rd ed., (Wiley-Interscience, 2004).
6. S. Paria, K.C. Khilar, *Adv. Colloid Interfac.* 110 (2004): p. 75-95.
7. R. Bordes, J. Tropsch, K. Holmberg, *Langmuir* 26 (2010): p. 3077-3083.
8. A. Sivakumar, P. Somasundaran, S. Thach, *Colloid Surface A* 70 (1993): p. 69-76.
9. A. Sivakumar, P. Somasundaran, S. Thach, *J. Colloid Interf. Sci.* 159 (1993): p. 481-485.
10. A. Sivakumar, P. Somasundaran, *Langmuir* 10 (1994): p. 131-134.
11. A.X. Fan, P. Somasundaran, N.J. Turro, *Langmuir* 13 (1997): p. 506-510.
12. R.K. Thomas, D.C. Mcdermott, G. Fragneto, *Abstr. Pap. Am. Chem. S.* 210 (1995): p. 193-COLL.
13. G. Fragneto, J.R. Lu, D.C. Mcdermott, R.K. Thomas, A.R. Rennie, P.D. Gallagher, S.K. Satija, *Langmuir* 12 (1996): p. 477-486.
14. S. Manne, J.P. Cleveland, H.E. Gaub, G.D. Stucky, P.K. Hansma, *Langmuir* 10 (1994): p. 4409-4413.
15. R. Atkin, V.S.J. Craig, E.J. Wanless, S. Biggs, *Adv. Colloid Interfac.* 103 (2003): p. 219-304.
16. X.H. Li, G.N. Mu, *Appl. Surf. Sci.* 252 (2005): p. 1254-1265.
17. P.M. Karlsson, M.W. Anderson, A.E.C. Palmqvist, *Corros. Sci.* 52 (2010): p. 1103-1105.
18. A. Imanishi, M. Suzuki, Y. Nakato, *Langmuir* 23 (2007): p. 12966-12972.
19. X.H. Cui, S.Z. Mao, M.L. Liu, H.Z. Yuan, Y.R. Du, *Langmuir* 24 (2008): p. 10771-10775.
20. C. Gutig, B.P. Grady, A. Striolo, *Langmuir* 24 (2008): p. 13814-13814.
21. C. Bellmann, A. Synytska, A. Caspari, A. Drechsler, K. Grundke, *J. Colloid Interf. Sci.* 309 (2007): p. 225-230.
22. N.R. Chevalier, C. Chevallard, P. Guenoun, *Langmuir* 26 (2010): p. 15824-15829.
23. S. Manne, H.E. Gaub, *Science* 270 (1995): p. 1480-1482.
24. J.F. Liu, G. Min, W.A. Ducker, *Langmuir* 17 (2001): p. 4895-4903.
25. C.E. Jhuma Das, S. Perkin, M.L. Berkowitz, *Langmuir* 27 (2011): p. 5.
26. R.D. Tilton, S.B. Velegol, B.D. Fleming, S. Biggs, E.J. Wanless, *Langmuir* 16 (2000): p. 2548-2556.
27. J.B. Valim, P.C. Pavan, E.L. Crepaldi, G.D. Gomes, *Colloid Surface A* 154 (1999): p. 399-410.
28. X.H. Li, S.D. Deng, G.N. Mu, H. Fu, F.Z. Yang, *Corros. Sci.* 50 (2008): p. 420-430.
29. P. Somasundaran, Q. Zhou, *J. Colloid Interf. Sci.* 331 (2009): p. 288-294.
30. L.C.d.M. Tania Farias, Jerzy Zajac, Aramis River, *J. Colloid Interf. Sci.* 363 (2011): p. 11.
31. Y. Chen, W.P. Jepsen, *Electrochim. Acta* 44 (1999): p. 4453-4464.
32. Y.G. Zheng, X. Jiang, W. Ke, *Corros. Sci.* 47 (2005): p. 2636-2658.
33. S.O. Saad Ghareba, *Corros. Sci.* 53 (2011): p. 8.
34. G. A. Schmitt, W. Bucken, R. Fanebust, *Corrosion* 48 (1992): p. 431-440.
35. E. Gulbrandsen, S. Nešić, A. Stangeland, T. Burchardtt, CORROSION/98, paper no. 13 (Houston, TX: NACE International, 1998).
36. G. Binnig, C.F. Quate, C. Gerber, *Phys. Rev. Lett.* 56 (1986): p. 930-933.
37. D.A. Lopez, S.N. Simison, S.R. de Sanchez, *Corros. Sci.* 47 (2005): p. 735-755.
38. S.W. Xia, M. Qiu, L.M. Yu, F.G. Liu, H.Z. Zhao, *Corros. Sci.* 50 (2008): p. 2021-2029.
39. J. Zhang, J.X. Liu, W.Z. Yu, Y.G. Yan, L. You, L.F. Liu, *Corros. Sci.* 52 (2010): p. 2059-2065.
40. E.S. Chan, B.B. Lee, P. Ravindra, *Colloid Surface A* 332 (2009): p. 112-120.
41. F. Anariba, S.H. DuVall, R.L. McCreery, *Anal. Chem.* 75 (2003): p. 3837-3844.
42. A. Noy, C.D. Frisbie, L.F. Rozsnyai, M.S. Wrighton, C.M. Lieber, *J. Am. Chem. Soc.* 117 (1995): p. 7943-7951.
43. Y. Choi, A. Magalhaes, F. Farelac, C. Andrade, S. Nešić, "Corrosion Behavior of Deep Water Oil Production Tubing Material Under Supercritical CO₂ Environment: Part I. Effect of Pressure and Temperature," CORROSION 2013, paper no. 2380 (Houston, TX: NACE, 2013).
44. S. Boufi, S. Alila, M.N. Belgacem, D. Beneventi, *Langmuir* 21 (2005): p. 8106-8113.
45. D. Asefi, M. Arami, A.A. Sarabi, N.M. Mahmoodi, *Corros. Sci.* 51 (2009): p. 1817-1821.
46. Y.G. Zheng, X. Liu, *Corros. Eng. Sci. Techn.* 43 (2008): p. 87-92.
47. T.G. Harvey, S.G. Hardin, A.E. Hughes, T.H. Muster, P.A. White, T.A. Markley, P.A. Corrigan, J. Mardel, S.J. Garcia, J.M.C. Mol, A.M. Glenn, *Corros. Sci.* 53 (2011): p. 2184-2190.
48. A. Döppenschmidt, B. Hans-Jürgen, *Langmuir* 16 (2000): p. 6709-6714.
49. L.C. Maley, W.P. Jepsen, *J. Energ. Resour.-Asme.* 122 (2000): p. 193-197.
50. G. Schmitt, M. Muller, G. Siegmund, "A Probabilistic Model for Flow Induced Localized Corrosion," CORROSION 2000, paper no. 49 (Houston, TX: NACE, 2000).
51. G.S. R. Hausler, "Hydrodynamic and Flow Effects on Corrosion Inhibition," CORROSION 2004, paper no. 4402 (Houston, TX: NACE, 2004).
52. D.J. S. Bosenberg, T. Becker, S. Bailey, R. De Marco, "Resolving the Structure of Carbon Dioxide Corrosion Inhibitors on Surfaces," Corrosion Control 07, paper no. 113 (Australasian Corrosion Association, 2007).
53. D. Turcio-Ortega, T. Pandiyan, J. Cruz, E. Garcia-Ochoa, *J. Phys. Chem. C* 2007, 111, 9853-9866.
54. S. Xia, M. Qiu, L. Yu, F. Liu, H. Zhao, *Corros. Sci.* 50 (2008): p. 2021-2029.